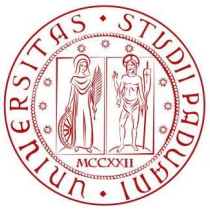

UNIVERSITÀ DEGLI STUDI DI PADOVA

Dipartimento di Fisica e Astronomia "Galileo Galilei"

Corso di Laurea in Fisica

Tesi di Laurea

Generazione e propagazione di fasci luminosi di caustiche

Generation and propagation of caustic beams of light

Relatore	Laureando
Dr. Gianluca Ruffato	Federico De Vidi

Anno Accademico 2023/2024

Abstract

Caustics are a widespread optical phenomenon occurring whenever a spatially variant interface perturbs the propagation of a light field. Under particular conditions, caustics can propagate in the form of beams with unique properties, such as self-healing and self-acceleration, revealing stable structured patterns of light with intriguing applications for life science and information and communication technology. In this thesis, we will consider the theory underlying the generation of a new kind of caustic beams, so-called polygon beams, and perform numerical simulations to investigate their properties and dynamics in the visible range. Diffractive optical elements will be fabricated using maskless optical lithography and characterized in the optical lab to analyze the generation and propagation of polygon caustic beams and compare experimental data with simulations.

Abstract

Le caustiche sono un fenomeno ottico diffuso che si verifica ogni volta che un'interfaccia variabile nello spazio perturba la propagazione del campo luminoso. Sotto particolari condizioni, le caustiche possono propagarsi nella forma di fasci con caratteristiche peculiari, come quella di auto-riparazione e di auto-accelerazione, rivelando pattern strutturati di luce stabili con affascinanti applicazioni per le scienze della vita e le tecnologie dell'informazione e della comunicazione. In questa tesi, verrà considerata la teoria alla base della generazione di un nuovo tipo di caustiche, i cosiddetti fasci poligonali, e saranno eseguite delle simulazioni numeriche per investigare le loro proprietà e la loro dinamica nello spettro del visibile. Elementi ottici diffrattivi saranno fabbricati usando la litografia ottica senza maschera e saranno caratterizzati nel laboratorio di ottica per analizzare la generazione e la propagazione di fasci di caustiche poligonali e confrontare i dati sperimentali con le simulazioni.

Contents

Introduction

Structured light aims to control the degrees of freedom of light fields, namely the intensity, the phase, and the orbital angular momentum. The development of structured light in the last 30 years has unveiled an ever increasing variety of light modes, organized in a vast zoology, with promising technological applications. One counterintuitive behavior encountered in several light beams is the optical self-healing, or self-reconstruction, that is the property of a beam of light to recover its structure after being obstructed by an opaque obstacle. It was initially observed in Bessel beams by MacDonald *et al* in 1996 [1], with circular obstacles subtracting the central spot, and by Boucahl *et al* in 1998 [2], who coined the term *self-healing*, by investigating this effect with more complex obstructions. Since then it has been observed in a large variety of light beams, largely enriched by the expansion of structured light. The fields that could benefit from self-healing of light are many, for instance optical communications [3], obstacle-circumventing micro-manipulation [4], or ghost imaging [5], to name but a few. To date the theoretical explanation to self-healing is still debated, and seems to originate from different physical properties depending on the beam where we find it, such as the property of non-diffraction, or that of self-acceleration [6]. Among the others, self-healing has also been observed in diffracting beams coupled with caustic structures, such as for instance the Airy beams [7], the Pearcey beams [8] or the Mathieu beams [9].

Caustics, on the other hand, are an optical phenomenon known and studied for centuries. They are patterns of high luminous intensity, and they find explanation in ray optics. They are indeed the envelope of rays reflected or refracted by a surface, namely the surface the rays arrive tangent to. Caustics can be found in the daily life for example when illuminating a cup from above, or in the patterns produced by the water surface in the bottom of a swimming pool, also rainbows are an example of this optical phenomenon. Recently a new variety of structured light presenting a caustic structure has been studied, the so-called polygon caustics, characterized by hypoycloids with accelerating cusps [10], showing the possibility to tailor their shape and intensity. Thanks to their ability to convey a great luminous intensity in confined regions, these beams can find numerous applications for example in micromachining [4] or in particle trapping and tweezing [11] or in high resolution microscopy [12]. Furthermore, in the recent years new technologies and techniques have been developed to structure light at the microscale and nanoscale. For example maskless lithography has enhanced the fabrication of diffractive optical elements(DOE), with the possibility to transfer complex height patterns on a small wafer.

The objective of this thesis is to study the generation and the propagation of the polygon caustic beams of light, and to test the limits of their ability of self-healing. The self-healing will be studied initially via simulations. To this aim a Matlab code has been written to simulate the propagation of the caustics, including the possibility of placing an obstacle along the propagation of the beam. The beams will be finally generated experimentally through diffractive optical elements, that will be fabricated with the technique of grayscale optical lithography. Finally the optical elements will be characterised with an experiment on the optical table to test their consistency with the simulations. The self-healing property will be then tested on the physical beams, and compared with the simulations.
The chapters are organized as follows:

- Chapter 1: The theoretical tools necessary to deal with a light beam that propagates after crossing a thin optical element, and how this can generate a caustic, are delineated. The attention

is then focused on those special lenses that allow the formation and propagation of polygon caustics, namely those generating circular-sector transformations (CST).

- Chapter 2: The property of self-healing in polygon beams is observed through numerical simulations, testing it for various obstacles. A parameter is then introduced to quantify the level of reconstruction achieved.
- Chapter 3: Fabrication of the diffractive optical elements through grayscale optical lithography with the machine for maskless optical lithography (uMLA, Heidelberg Instruments). Later on, the characterization of the optical elements will be carried out with an experiment on the optical table, and the obstruction of the physical beam will be tested, generating obstacles with a spatial light modulator (SLM).

Chapter 1

Free-space propagation: theory and simulations

1.1 Fourier optics and convolution algorithm

When an electromagnetic wave propagates in a linear, homogenous, non-dispersive and isotropic medium we can derive from Maxwell's equations the light wave equation, for example for the electric field $\vec{E}(\mathbf{r},t)$ of a wave propagating in vacuum:

$$\nabla^2\vec{E}(\mathbf{r},t) - \frac{1}{c^2}\partial_t^2\vec{E}(\mathbf{r},t) = 0 \tag{1.1}$$

where c is the speed of light in vacuum. Since in such a case every component of the electromagnetic field follows its own equation, uncorrelated to the others, we can use the scalar diffraction theory, and describe one component of the wave with a complex field. We can further require the wave to be monochromatic, i.e. to have a fixed amplitude in every point in space that oscillates with a certain frequency:

$$U(\mathbf{r},t) = U(\mathbf{r})exp(-i\omega t + \varphi_0(\mathbf{r})) \tag{1.2}$$

seeking monochromatic waves solutions for the wave equation leads to the Helmholtz equation:

$$\nabla^2 U + k^2 U = 0 \tag{1.3}$$

The application of Green's theorem with a spherical monochromatic wave as Green's function to the Helmholtz equation leads to the theorem of Helmholtz and Kirchhoff [13]. This theorem allows the evaluation of the field inside a closed surface over which the field is known. Let us consider a beam incident on an aperture that lays on a plane, or alternatively, a wave whose magnitude decreases rapidly on this plane, as it happens for a Gaussian beam produced by a laser. By imposing the Kirchhoff boundary conditions to a suitable surface containing the point of interest, the Helmholtz-Kirchhoff theorem allows to calculate the value of the field at a given point in the side of the plane opposite to that of the source of the wave, consequently it is possible to evaluate the field on a plane at a certain distance from the aperture [13]. The solution to this problem gives the Fresnel-Kirchhoff diffraction formula:

$$U(\mathbf{s}) = \frac{1}{i\lambda}\iint_S U_i(\mathbf{r})\,\frac{e^{ik\sqrt{(\xi-x)^2+(\eta-y)^2+z^2}}}{\sqrt{(\xi-x)^2+(\eta-y)^2+z^2}}\,d\xi\,d\eta \tag{1.4}$$

where $\mathbf{r}$=(ξ,η) are the coordinates of the input plane, while $\mathbf{s}$=(x,y) are the coordinates of the arrival plane, and S is the surface containing the aperture, or the region where the field is different from 0, as shown in figure (1.1). In paraxial regime the complex term can be approximated to the second order,

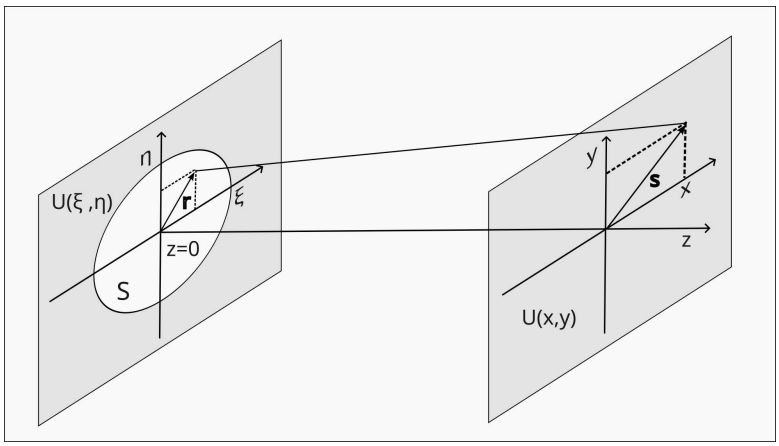

Figure 1.1: Reference frame adopted in the diffraction integrals

obtaining the Fresnel integral that will be used to propagate the field from a transversal section to the other along the optical axis:

$$U(x,y) = \frac{e^{ikz}}{i\lambda z} \iint_S U_i(\mathbf{r})\, e^{i\frac{k}{2z}|\mathbf{r}-\mathbf{s}|^2}\, d\mathbf{r} \tag{1.5}$$

Introducing the function:

$$h(\mathbf{r}) = \frac{e^{ikz}}{i\lambda z} e^{i\frac{k}{2z}r^2} \tag{1.6}$$

the field in the arrival transverse plane is proportional to the Fourier transform of $A(\mathbf{r}) = U(\mathbf{r})h(\mathbf{r})$. From another point of view the Fresnel integral can be treated as a convolution operation between the field that is propagating $U(\mathbf{r})$ and $h(\mathbf{r})$ that is now treated as an impulse response function.

$$U(\mathbf{s}) = U(\mathbf{r}) * h(\mathbf{r}) \tag{1.7}$$

To evaluate the field we can thus use the convolution algorithm, implemented extensively whenever the output of a linear system has to be computed [14]:

$$U(\mathbf{s}) = \mathcal{F}^{-1}\left[\mathcal{F}(U(\mathbf{r})) \cdot \mathcal{F}(h(\mathbf{r}))\right] \tag{1.8}$$

where $H = \mathcal{F}(h(\mathbf{r}))$ is the transfer function. The Matlab software written for the propagation of the field will use this algorithm. The approach is then to discretize the field over a squared surface and using the fast Fourier transform (FFT) to evaluate (1.7), and simulate the propagation of light. Numerically the algorithm can be carried out in two different regimes, namely the transfer function propagator (TF) and the impulse response propagator (IR). For the TF, the analytical expression of H is discretized in (1.7), while for the IR, $\mathcal{F}(h(r))$ is evaluated numerically with the FFT. These two methods are analytically equivalent, but required in order to meet the Nyquist sampling theorem in the simulations for a particular choice of pixel number and size, in particular to avoid under-sampling, that would lead for example to sharp spikes in the TF regime, or the periodic repetition of the image in the IR regime [15]. For the TF regime the correct sampling or the oversampling are achieved if $\Delta x \leq \frac{\lambda z}{L}$, for the IR regime if $\Delta x \geq \frac{\lambda z}{L}$.

1.2 Conformal transformations

Let us now consider a monochromatic wave incident on a thin layer made of a transparent material, that doesn't absorb energy from the beam, with a refractive index different from that of the propagation

medium. The field at each point over the plane immediately after the optical element will have the same amplitude as the field on the plane directly in front of it, but with a phase difference that depends locally on the thickness of the material being crossed:

$$U_t(\mathbf{r}) = U_i(\mathbf{r}) \cdot t(\mathbf{r}) \tag{1.9}$$

$$t(x,y) = e^{i\Omega(x,y)} \tag{1.10}$$

where $\Omega(x,y)$ is the phase shift locally induced by the optical element, U_i is the input field, U_t is the output field, and t is the transmission function. In this study the Fresnel-Kirchhoff diffraction formula is used to propagate the field after it has been refracted by a thin optical element. The calculations can be simplified using the stationary phase approximation(SPA) [16], that states that an integral of a rapidly oscillating function can be approximated by the sum of the values of the integrand at the saddle points of its phase (x^*, y^*), leading to the following expression [10]:

$$U_z(\mathbf{s}) = \sum_{\mathbf{r}^*} \frac{2\pi\sigma}{\lambda z} e^{i\lambda z} \frac{U(x^*,y^*)}{\sqrt{|H|}} e^{i\Phi(x^*,y^*)} \tag{1.11}$$

$$\Phi(x,y) = \Omega(x,y) + \frac{k}{2z}\left|\mathbf{r}-\mathbf{s}\right|^2 - \frac{k}{2f}\left|\mathbf{r}\right|^2 \tag{1.12}$$

here $\mathbf{r}$=(ξ,η) and $\mathbf{s} = (x,y)$ are respectively the coordinates of the departure and arrival plane, $H = AB - C^2$ is the determinant of the Hessian of $\Phi(x,y)$, with $A = \Phi_{xx}$,$B = \Phi_{yy}$,$C = \Phi_{xy}$, and σ is the sign of H if its first element A is a positive number, otherwise it's equal to $-i$. Furthermore in the phase a focal term was included, with focal length f.
The SPA is a zero order approximation, and it ultimately allows to treat the problem with geometric optics, as if from every point of the plane a ray would leave with a certain angle and carrying a certain energy density [10], [17]. This approach also establishes a map $\mathbf{s}(x,y)$ between the points of the two planes, since the stationary points are found requiring:

$$\nabla\Phi(x,y) = \nabla\Omega(x,y) + k\left\{\left(\frac{1}{z}-\frac{1}{f}\right)\mathbf{r} - \frac{1}{z}\mathbf{s}\right\} = 0 \tag{1.13}$$

it is convenient to solve for $z = f$, so that now $\mathbf{s}$ are the coordinates on the focal plane:

$$\nabla\Omega(x,y) = \frac{k}{f}\mathbf{s} \tag{1.14}$$

For this experiment we require the transformation $s(x,y)$ to be conformal, meaning that it locally conserves the angles between intersecting curves. This in general is equivalent to require that $s(x,y) = [u(x,y)\ v(x,y)]$ satisfies the Cauchy-Riemann conditions:

$$\frac{\partial u}{\partial x} = \mp\frac{\partial v}{\partial y} \tag{1.15}$$

$$\frac{\partial u}{\partial y} = \pm\frac{\partial v}{\partial x} \tag{1.16}$$

That is to say that the function has to be either holomorphic or anti-holomorphic. Equation (1.14) implies that $\mathbf{s}$ is irrotational, and, as a consequence of equations (1.15,16), that it has to be anti-holomorphic. Moreover, a complex function $g\left(\overline{\zeta}\right)$ such that $[Re(g)\ Im(g)] = [u\ v]$, can be associated to $\mathbf{s}(x,y)$. The phase pattern needed to reproduce this transformation can be found integrating the following formula obtained from (1.14), with respect to $\overline{\zeta}$ [10]:

$$\partial_{\overline{\zeta}}\Omega = \frac{k}{2f}g \tag{1.17}$$

being $\partial_{\overline{\zeta}}$ the Wirtinger operator. Therefore, starting from a given transformation g it is possible to utterly describe the propagation of the field and the phase shift that the optical element has to impart

to the input beam. In this thesis the n-folds circular-sector transformation (CST) is considered [16], that transforms a circular sector of the input plane into a circumference in the arrival plane. Indeed, calling $\{r, \theta\}$ the coordinates of the input plane and $\{\rho, \varphi\}$ those of the arrival plane, the CST acts as:

$$\varphi = n\theta \qquad (1.18) \qquad\qquad \rho = a\left(\frac{r}{b}\right)^{-n} \qquad (1.19)$$

we can find the complex associated function g, and the phase pattern integrating equation (1.17) [10]:

$$g\left(\overline{\zeta}\right) = a\left(\frac{\overline{\zeta}}{b}\right)^{-n} \tag{1.20}$$

$$\Omega(r,\theta) = k\frac{ab}{f}\left(\frac{r}{b}\right)^{1-n}\frac{cos((1-n)\theta)}{1-n} \tag{1.21}$$

As we can see n-folds circular sector transformations are characterized by four parameters $\{f, n, a, b\}$. Where f,a,b are real positive numbers, and n is an integer different from 0 and 1.

1.3 Caustics generated from circular-sector transformations

A caustic, as it is conceived in geometric optics, is the envelope of the rays being reflected or refracted by an interface, namely it is the geometrical locus the rays arrive tangent to. For the Gaussian beam refracted by the optical element used in this study, the caustic could be thought of as a surface in the 3D space, or as a curve in the 2D plane where the beam is been propagated [17]. Over the points of a caustic, ray optics predicts the divergence of the field's magnitude. Indeed, if a group of rays leaving from an extended zone of the lens surface is concentrated in a very narrow area in the arrival plane, in this small region they convey a great luminous intensity, leading to the divergence of the field [17], [18]. Likewise, operating with conformal transformations, if in (1.11) we require H to be zero, in these points the field rises to infinity and the caustic skeleton forms. Solving for $H(x, y; z) = 0$ for a general transformation furnishes in the first place a relation between the coordinates in the input plane and the values of z for which the caustic forms in the following form:

$$H = AB - C^2 = 0 \rightarrow z_{\pm} = \frac{f}{1 \pm \left|g_{\overline{\zeta}}\right|} \tag{1.22}$$

with $A = \Phi_{xx}$,$B = \Phi_{yy}$,$C = \Phi_{xy}$. Inverting (1.22) we can also find the radius as a function of $z_{\pm}$:

$$r = b\left(\pm|n|\frac{a}{b}\frac{z_{\pm}}{f - z_{\pm}}\right)^{\frac{1}{n+1}} \tag{1.23}$$

substituting inside equation (1.13) the equations (1.22,1.14) leads to:

$$\mathbf{s}_{\pm} = \frac{\mathbf{s}_0 \pm \left|g_{\overline{\zeta}}\right|\mathbf{r}}{1 \pm \left|g_{\overline{\zeta}}\right|} \tag{1.24}$$

$$\mathbf{s}_0 = [Re(g)\ Im(g)] = |g|\,[cos(\theta_0)\ sin(\theta_0)] \tag{1.25}$$

where $\{r_0, \theta_0\}$ and $\mathbf{s}_0$, are respectively the polar and Cartesian coordinates on the focal plane, $\{r, \theta\}$ and $\mathbf{r}$ those of the optical element plane, and $\mathbf{s}$ is the parametric curve of the caustic on the plane at distance z. We can generate caustics in this fashion from circular sector transformations for which $\left|g_{\overline{\zeta}}\right| = |n|\frac{a}{b}\left(\frac{r}{b}\right)^{-n-1}$, $|g| = a\left(\frac{r}{b}\right)^{-n}$, and $\theta_0 = n\theta$, so that substituting this quantities in equations (1.24) and (1.25), and then substituting (1.25) in (1.24) we get:

$$\mathbf{s}_{\pm} = \gamma_{\pm}(r)[cos(n\theta) \pm |n|cos(\theta)\ sin(n\theta) \pm |n|sin(\theta)] \tag{1.26}$$

$$\gamma_{\pm}(r) = \frac{a(r/b)^{-n}}{[1 \pm |n|a/b(r/b)^{-n-1}]} \tag{1.27}$$

we can furthermore express (1.26) in polar coordinates obtaining:

$$\rho_{\pm}(z,\theta) = \frac{az_{\pm}}{f}\left(\frac{z_{\pm}\,|n|\,a}{b(z_{\pm}-f)}\right)^{-\frac{n}{n+1}}\sqrt{1+n^2 \pm 2\,|n|\,cos((1-n)\theta)} \tag{1.28}$$

Equation (1.28) also shows how the rays map a circumference lying on the lens plane into two different caustics for two values of z. In particular, for each circumference of radius r illuminated in the lens plane, two caustics are formed in two different planes, one before, and one after the focal length. The curves produced for a negative n are hypocycloids with $|n-1|$ cusps, while for positive n, we observe epicycloids with $n-1$ cusps [10].

In this thesis the reconstruction of hypocycloids for distances beyond the focal length is studied. Through the simulation carried out with the exact Fresnel integral we don't obtain the infinite intensities predicted by ray optics. Nevertheless, we obtain a curve characterized by a high intensity and a non-zero thickness overlapped to the theoretical caustic curve, that predicts with accuracy the shape and dimension of the beam. In the center of this region there is a bright area, while externally the field is characterized by a lower intensity. A caustic, in catastrophe theory [18], is indeed also the surface that separates two zones with different numbers of intersecting rays [17], and the internal points are reached by a greater number of rays. In the following images are presented several examples of the phase patterns for the CST, the beam propagated after the focal length, and the theoretical caustics super-imposed to the field. In particular, for the simulations the light fields have been discretised over squared grids of side-length $L = 6.8$ cm divided in 4800x4800 pixels, so that a single pixel has a 14 μm side-length. Other key parameters for the simulation, that characterise the input Gaussian beam, are the wavelength $\lambda = 632.8$ nm, and the waste $w_0 = 2.5$ mm. These parameters have been adopted thereon also for the simulations in the following chapters. It is worth noting the formation of $(1-n)$ cusps, distributed over a regular polygon expanding during beam propagation:

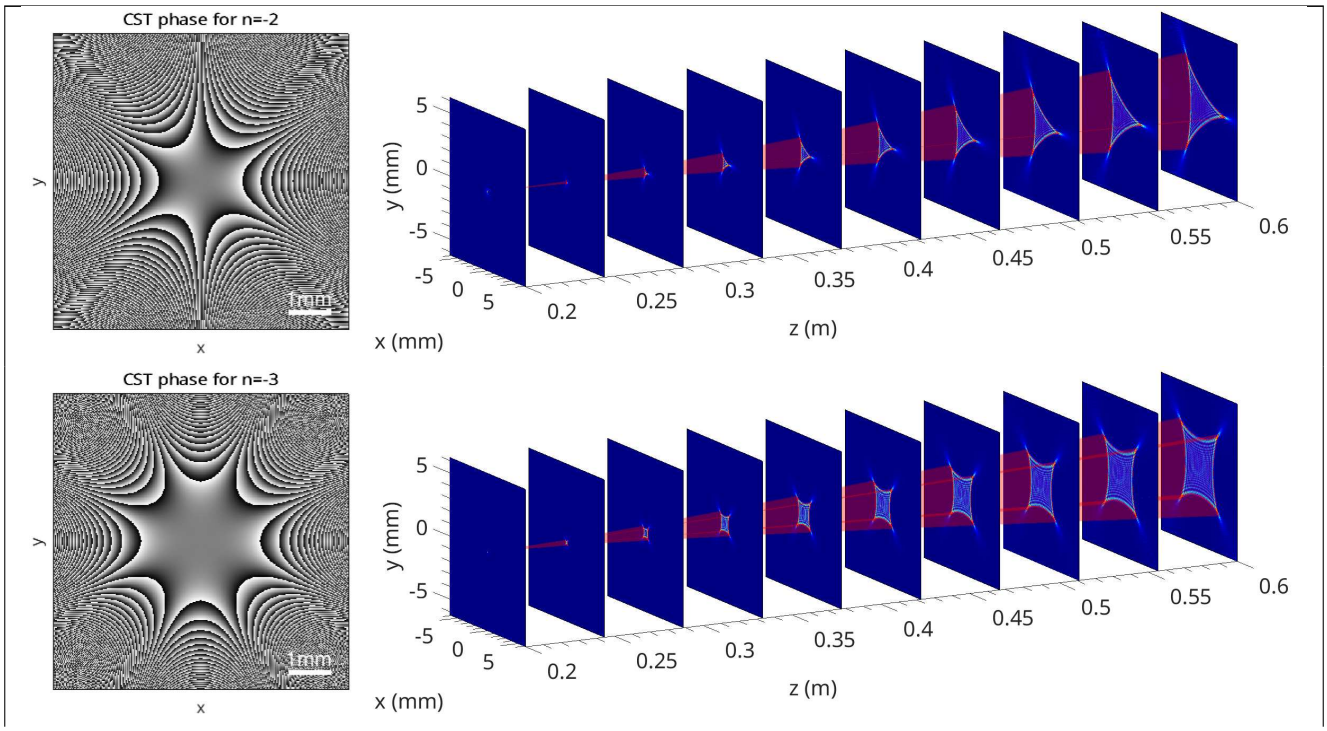

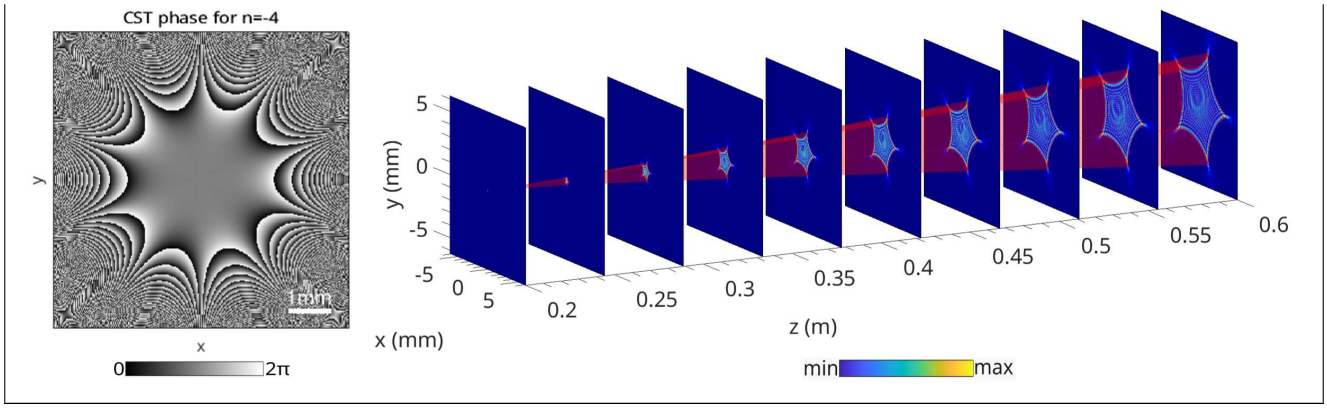

Table 1.1: propagation of several caustic beams through a CST transformation, the focal term $-kr^2/2f$ has been omitted to appreciate the phase given by (1.21). The transformation parameters are: $a = 2$ mm, $b = 3$ mm, $f = 20$ cm, and $n = -2$ for the image on the top, $n = -3$ for the central one, and $n = -4$ for the one in the bottom.

Chapter 2

Self-healing property of caustic beams

When a light beam encounters an obstacle along its propagation, generally its shape is rather distorted from the one we'd observe if no perturbation took place. Nevertheless, there are several beams that seem to recover their structure after being perturbed by an obstacle, ideally, as if no obstruction was encountered. Such beams are said to possess the property of self-healing. This property assumes importance in fields such as communication, where a modern challenge is making a space multiplexed beam travel for a long distance with a minimal modification of the beam phase and amplitude, especially when travelling in inhomogeneous media [19]. For instance the Airy [7] beams and the Mathieu [9] beams are known to behave in this way. Considering a case closer to our study, self-reconstruction was observed also in caustics generated by illuminating an axicon with a Gaussian beam [20]. In this case the self-healing was explained through ray optics, and the fact that the rays forming the caustics where conical and converging, enabling them to avoid an obstacle placed earlier than the caustic in the propagation axis.
In this chapter the obstructed propagation of caustic beams is simulated. We want to observe in detail whether also polygon caustic beams, as it is predicted in general for caustic beams, possess the self-healing property, and we want to study its limits. We'll focus mainly on beams with low number of cusps, namely the deltoid with three cusps and the astroid with four cusps.

2.1 Simulations of reconstruction

The approach that will be used to test the limits of self-healing is to consider and select obstacles of increasing size, from a small perturbation of the field, up to an obstacle of intermediate dimension, to an obstruction for which the structure of the beam is evidently disrupted, as the information subtracted doesn't allow its reconstruction. It will be observed qualitatively the level of regeneration of the beam during the propagation, from short to long distances, for which the shape of the beam is basically consolidated. Firstly, angular obstructions positioned on the cusp region will be considered:

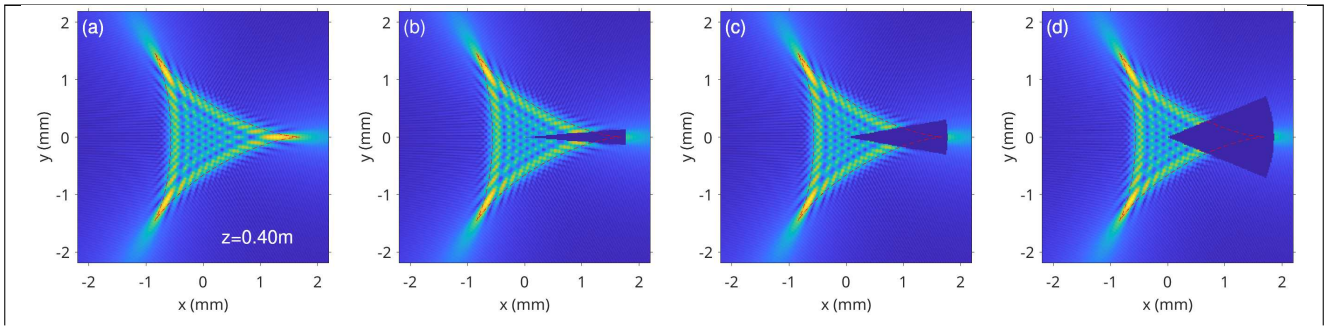

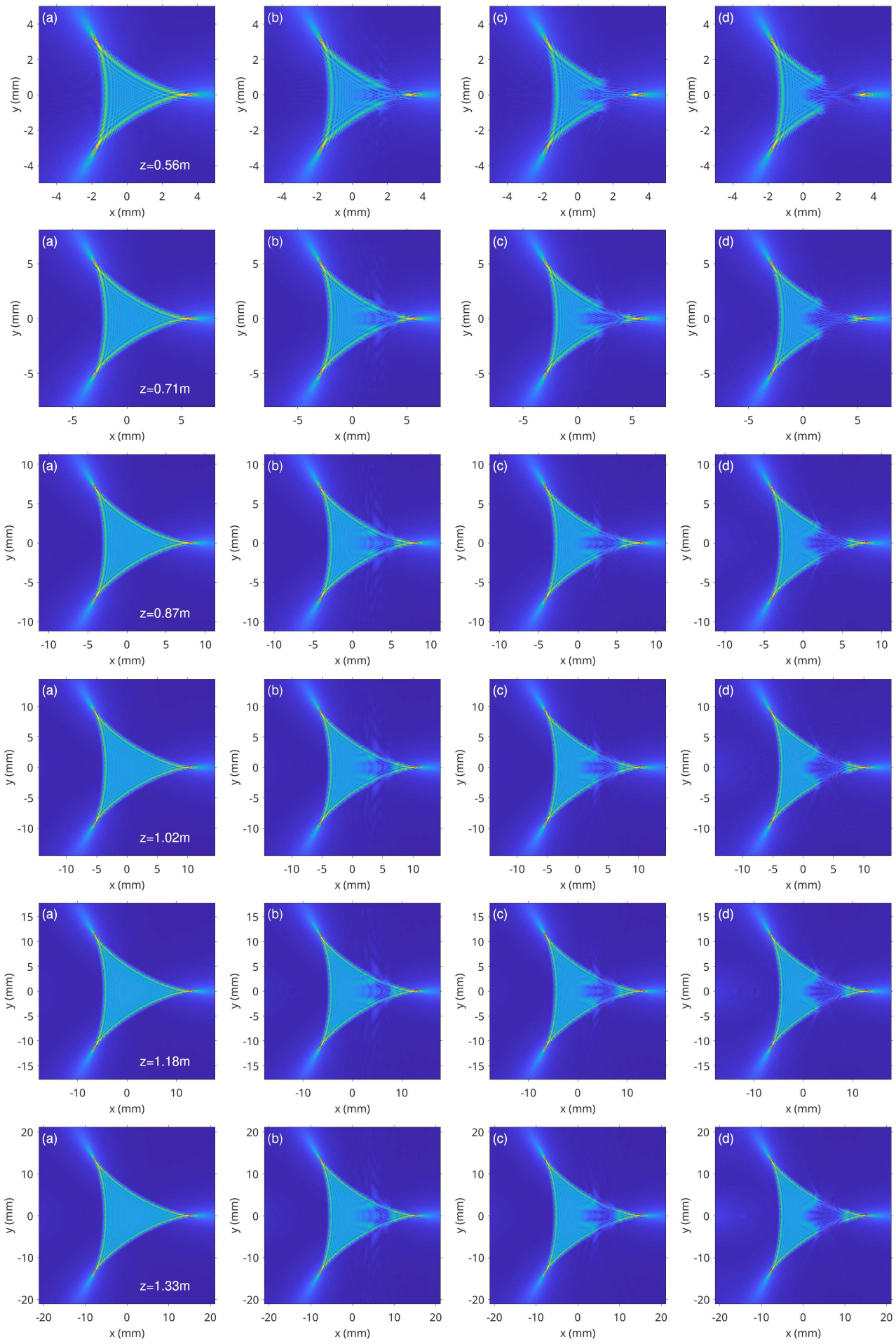
(a)
(b)
(c)
(d)
z=0.56m
z=0.71m
z=0.87m
z=1.02m
z=1.18m
z=1.33m
x (mm)
y (mm)

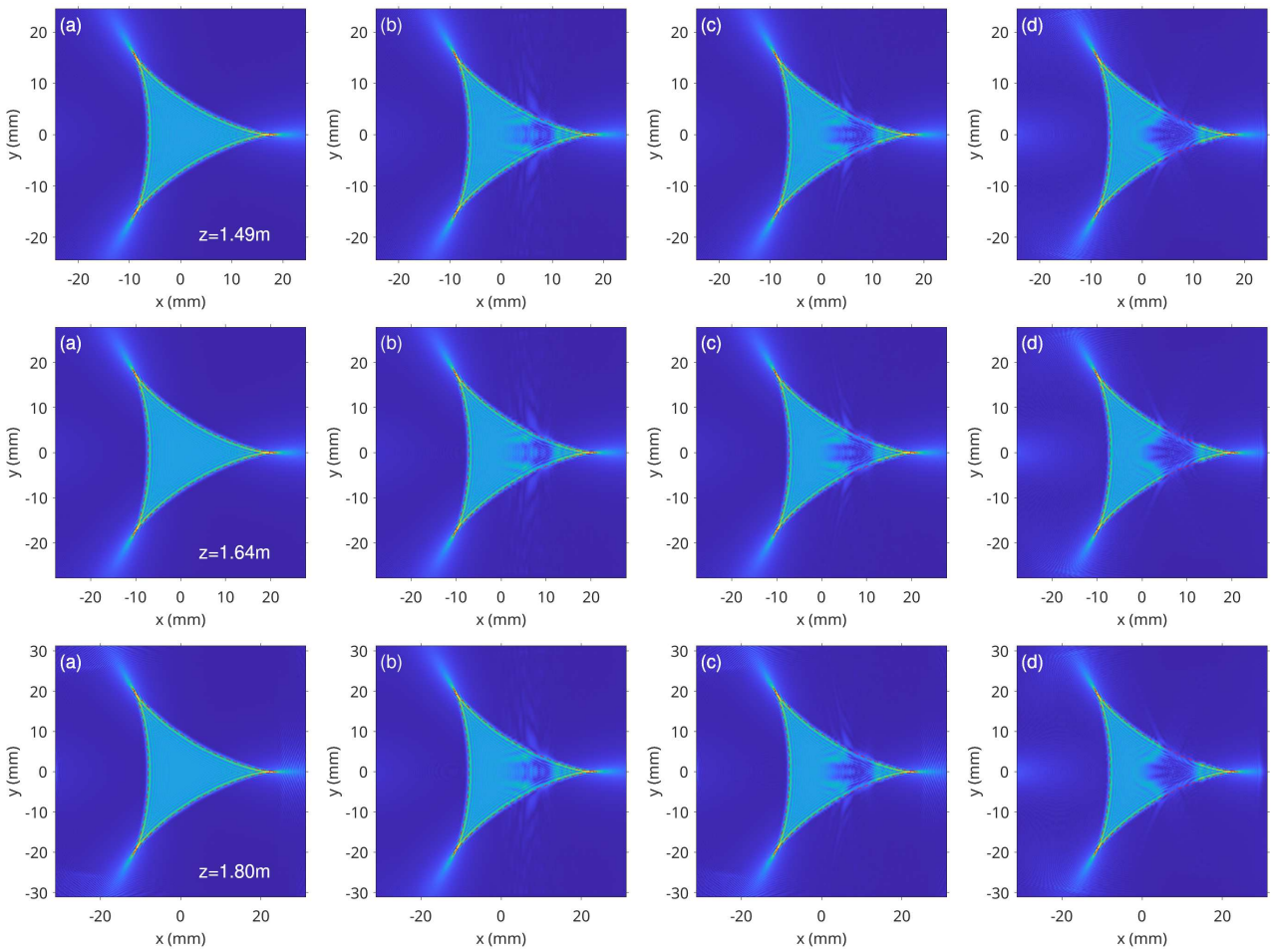

Obstacles

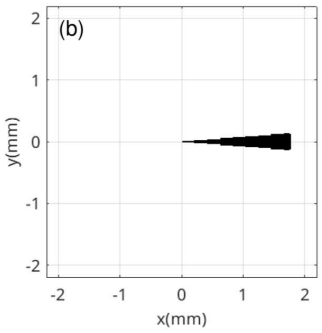

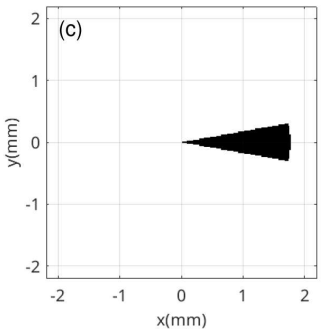

Space propagation

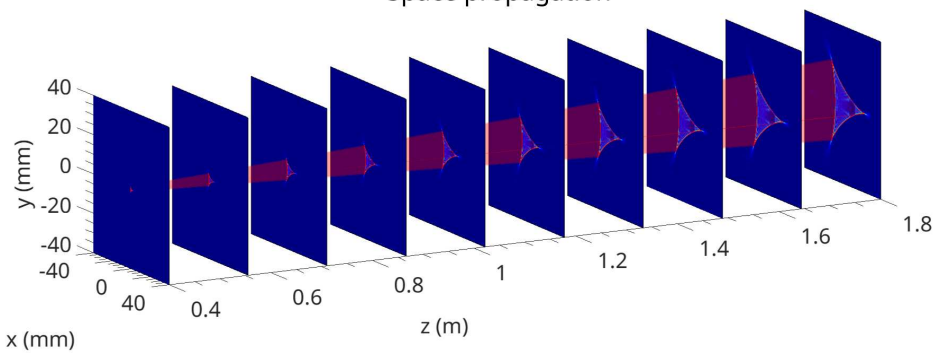

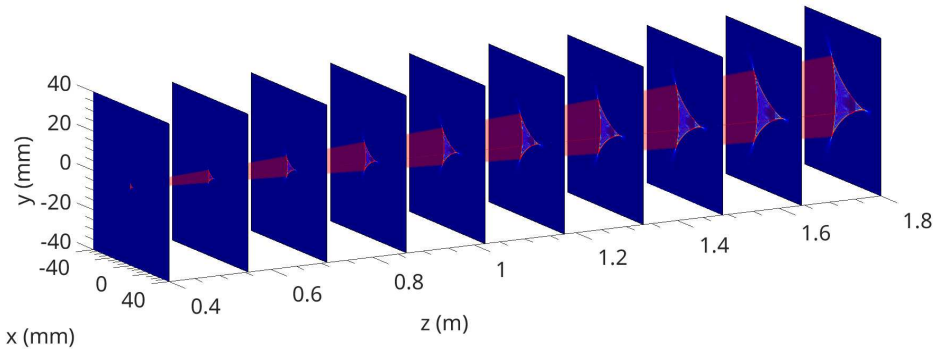

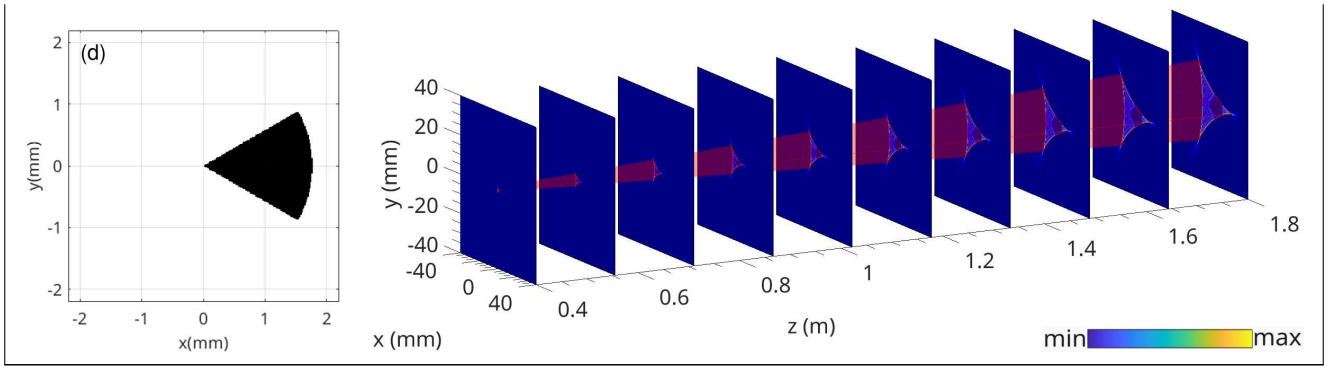

Table 2.1: (a) the unobstructed beam with parameters $n = -2$, $f = 20$ cm, $a = 2$ mm, $b = 3$ mm. The beam is propagated from $z = 2f$ to $z = 9f$ by equally spaced planes. This beam is compared with three obstructed beams with angular obstacles, all having the same radius $r = 1.76$ mm, and an increasing angle (b) $\theta = \pi/20$,(c) $\theta = \pi/9$ and (d) $\theta = \pi/3$.

The reconstruction in this case is influenced mainly by the amplitude of the obstacle for the inner bright region, while the zone around the cusp reappears identical to the unobstructed case. This can be explained again with the ray optics model, indeed the rays that end up building the cusp lay externally to the caustics, and are not blocked by the angular obstacles as shown in figures (2.1, 2.2). The reconstruction for this region is thus influenced also by how far the obstacle extends outside of the caustic, and obstructions with smaller radius lead to a better healing. Now circular obstacles are considered:

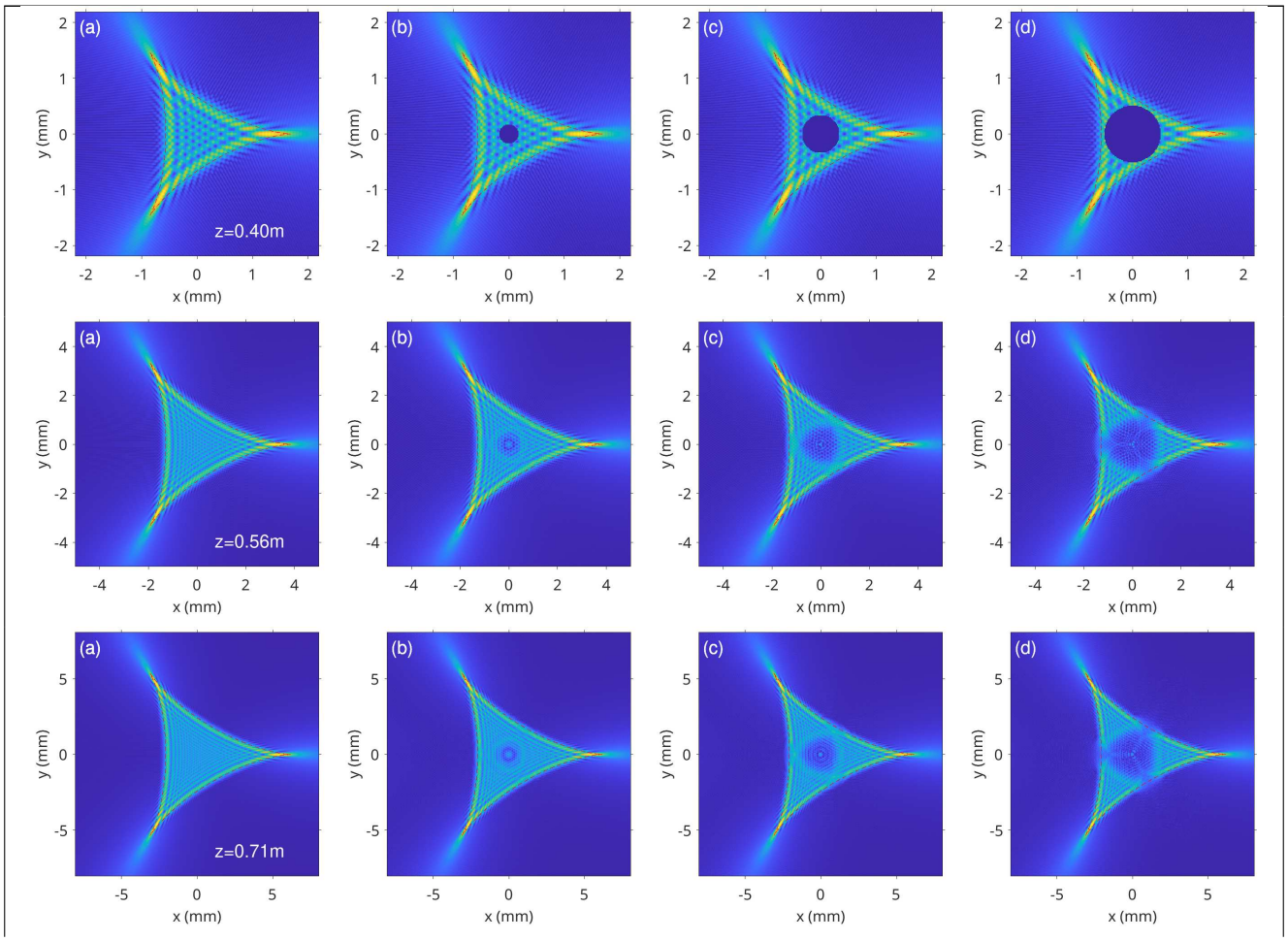

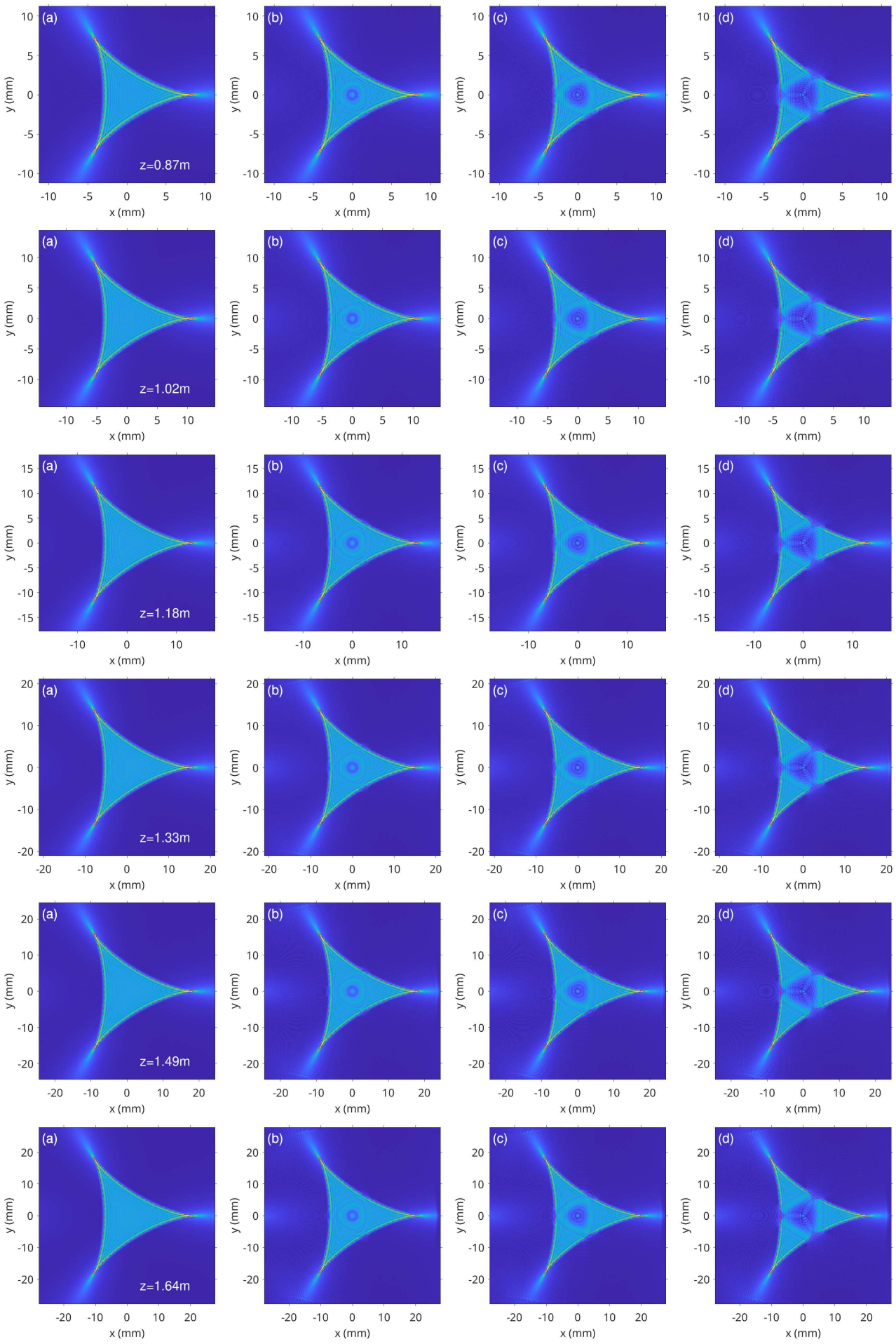
(a)
(b)
(c)
(d)
z=0.87m
z=1.02m
z=1.18m
z=1.33m
z=1.49m
z=1.64m
x (mm)
y (mm)

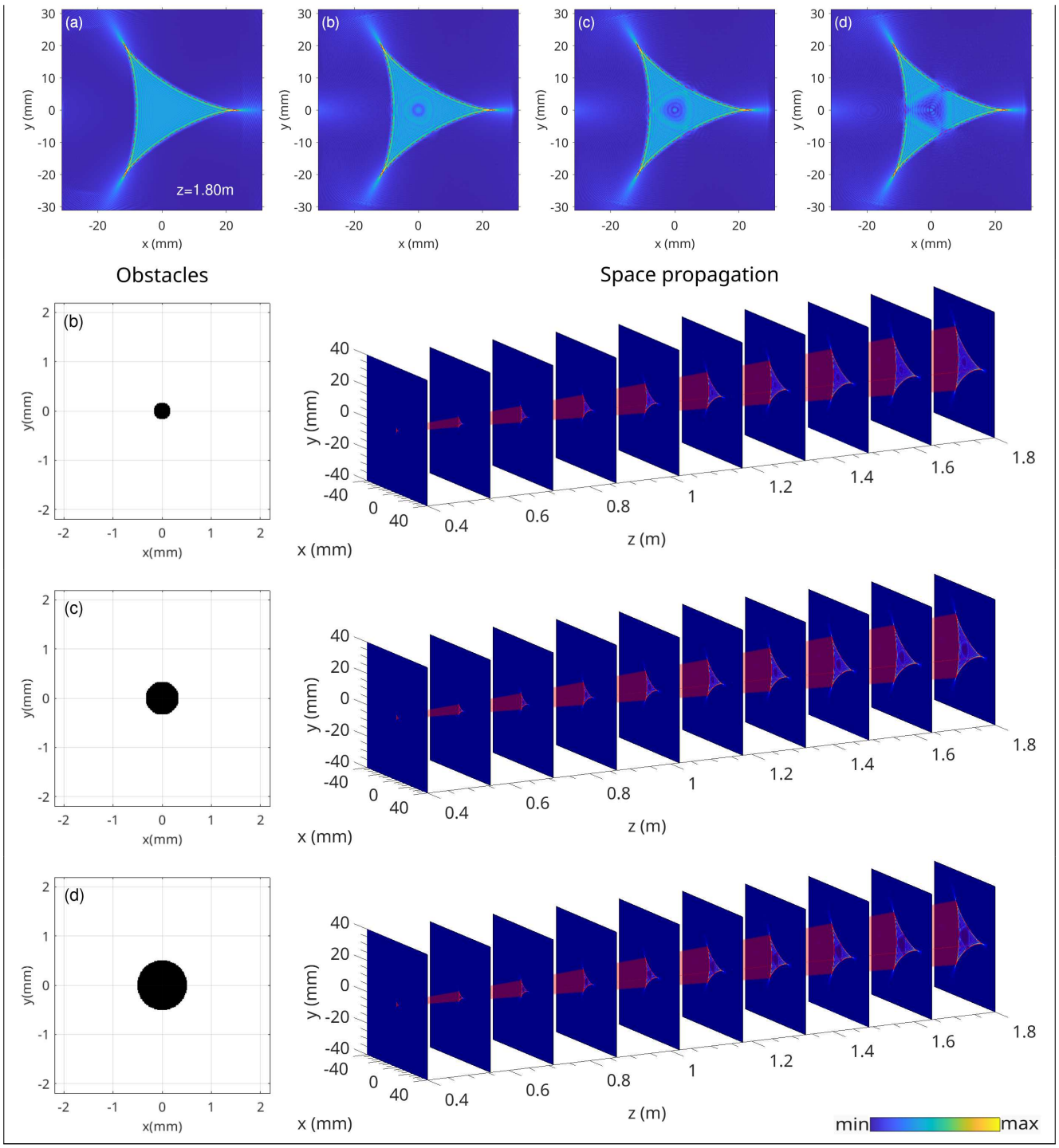

Table 2.2: (a) the unobstructed beam with parameters $n = -2$, $f = 20$ cm, $a = 2$ mm, $b = 3$ mm. The beam is propagated from $z = 2f$ to $z = 9f$ by equally spaced planes. This beam is compared with three obstructed beams with circular obstacle (b) $r = 0.17$ mm,(c) $r = 0.34$ mm and (d) $r = 0.50$ mm.

For circular obstacles the internal region passes from small perturbations, consisting in altering the shape of the internal fringes, to the formation of a dark region inside the caustic for big obstacles. An angular obstacle is now subtracted from a fold of the caustic.

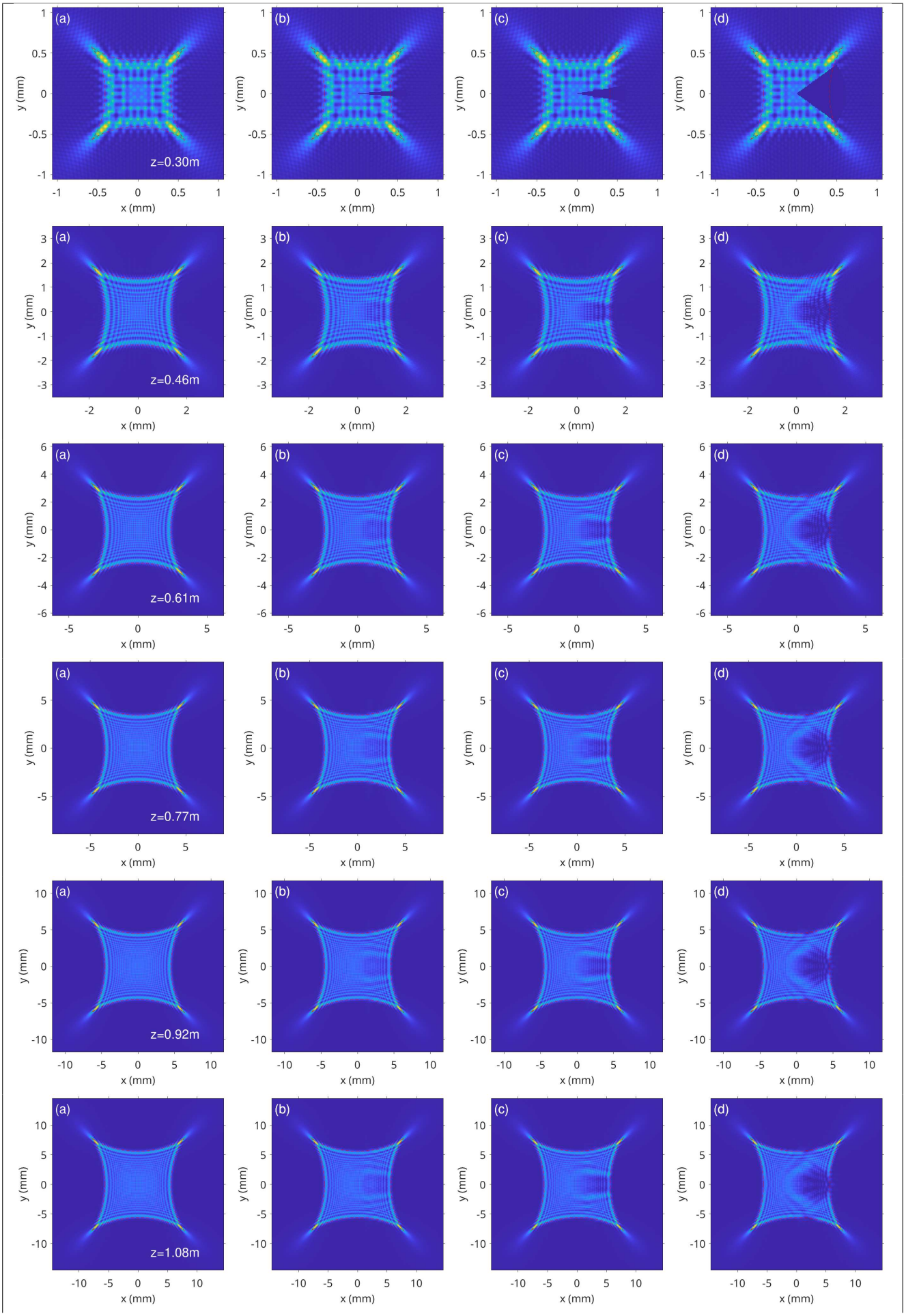
(a)
(b)
(c)
(d)
z=0.30m
z=0.46m
z=0.61m
z=0.77m
z=0.92m
z=1.08m
x (mm)
y (mm)

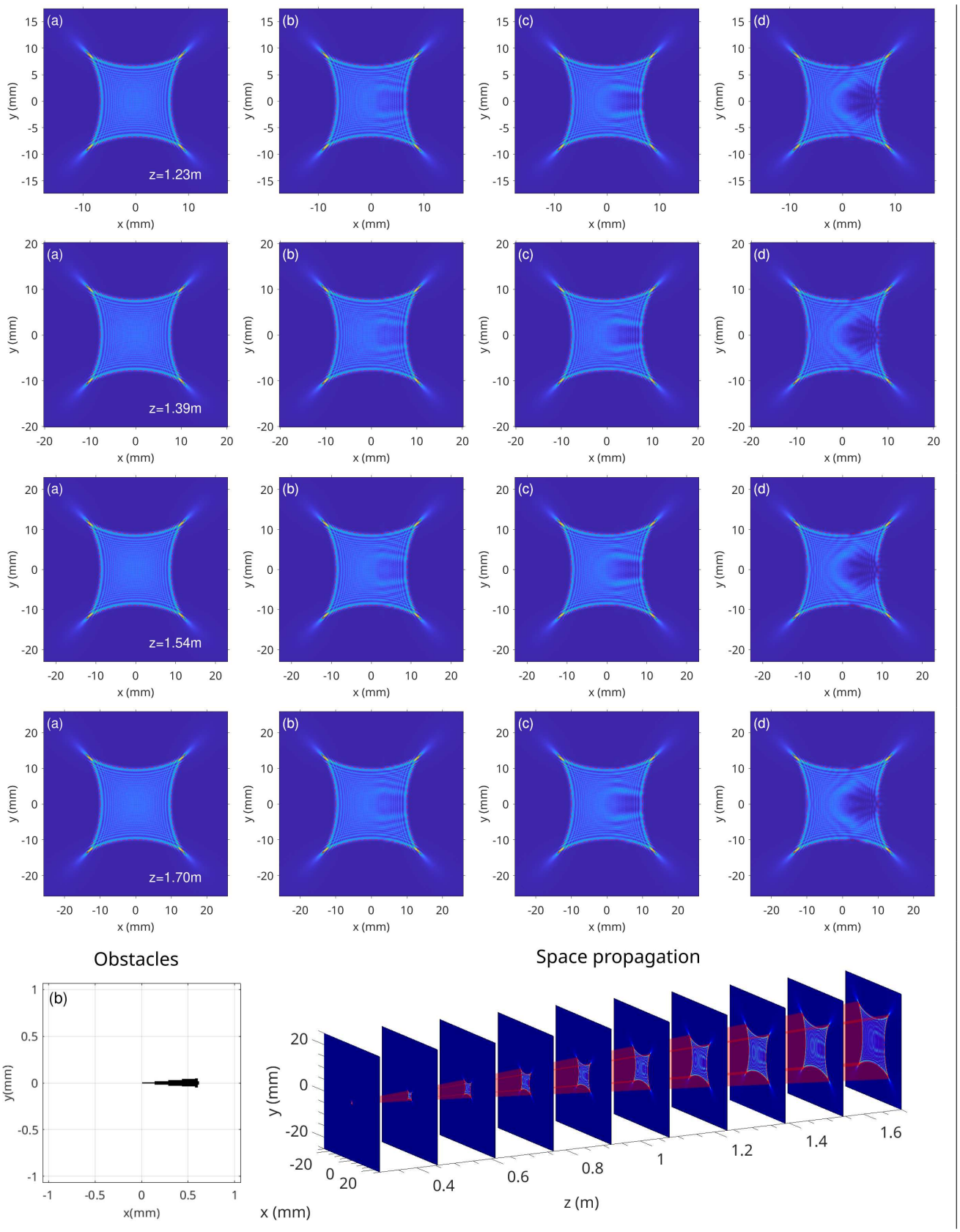
(a)
(b)
(c)
(d)
z=1.23m
z=1.39m
z=1.54m
z=1.70m
x (mm)
y (mm)
Obstacles
(b)
x(mm)
y(mm)
Space propagation
x (mm)
y (mm)
z (m)

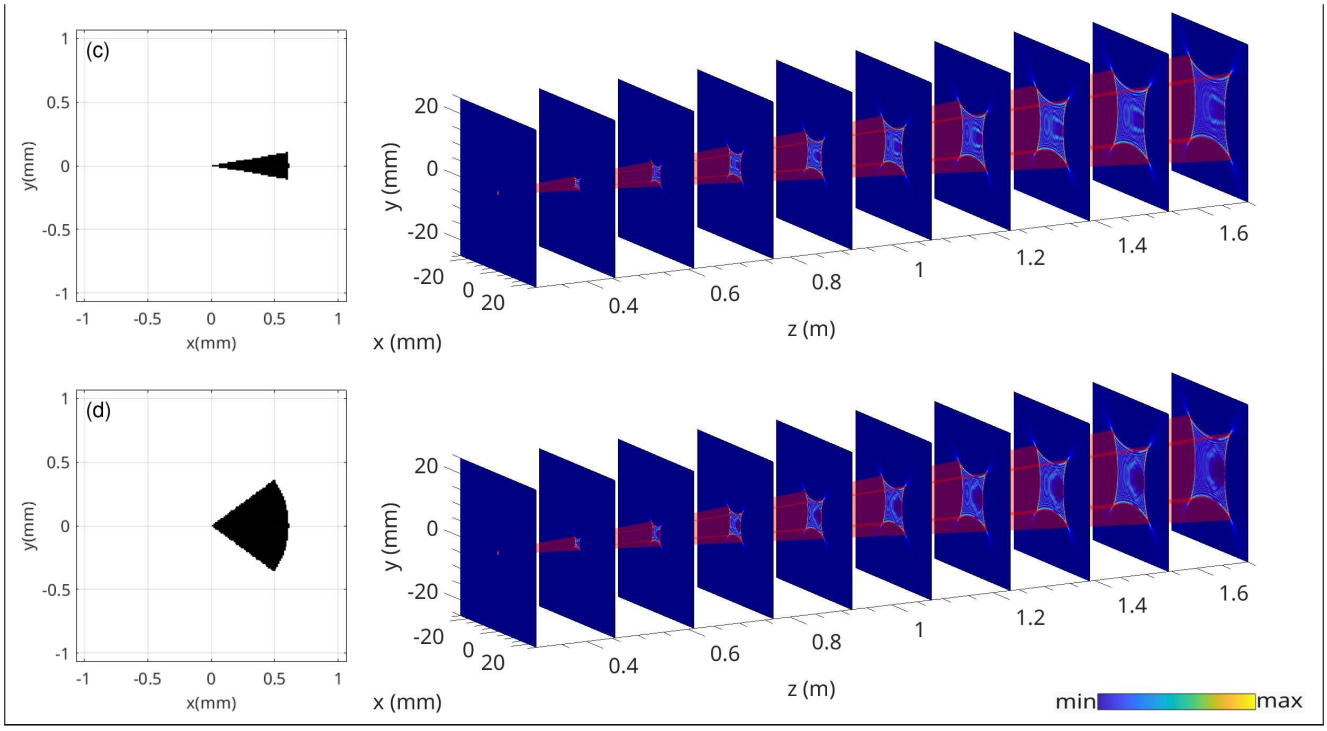

Table 2.3: (a) the unobstructed beam with parameters $n = -3$, $f = 20$ cm, $a = 2$ mm, $b = 3$ mm. The beam is been propagated from $z = 2f$ to $z = 9f$ by equally spaced planes. This beam is compared with three obstructed beams with angular obstacles, all having the same radius $r = 0.65$ mm, and an increasing angle (b) $\theta = \pi/20$,(c) $\theta = \pi/9$ and (d) $\theta = \pi/3$.

For this case the region along the caustic line regenerates better, as for the case of the angular obstacle placed on the cusp. The regeneration in this case is not affected by the extension of the beam outside the caustic, as the rays that form this part travel internally to the caustic surface, similarly to what happens for the folds in the following figures.
In all these cases it's been observed that the caustic has recovered its structure for obstacle of considerable sizes.

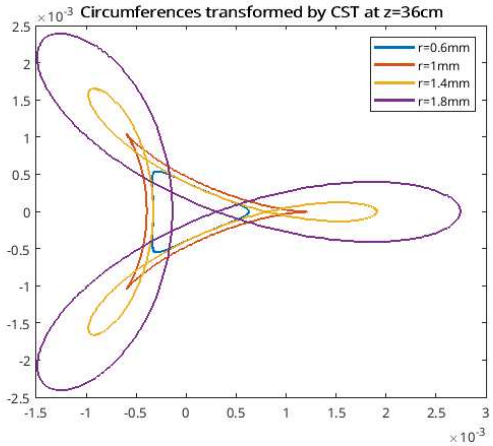

Figure 2.1: Transformation of circles of increasing radius mapped by a CST in a plane at distance $z = 36$ cm. The caustic is formed for $r = 1$ mm.

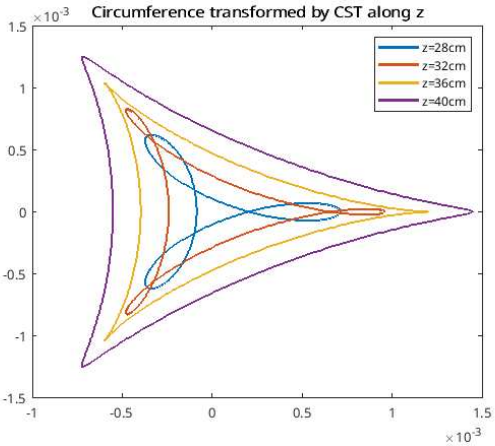

Figure 2.2: Transformation of a circle of radius $r = 1$ mm mapped by a CST at increasing values of z. The caustic is formed for $z = 36$ cm.

2.2 The reconstruction parameter

In the previous section we have discussed the reconstruction of the beams using a qualitative approach. In particular, we looked at the beam reconstructed and obstructed side by side to tell to what degree the beam recovered its structure as a function of distance, and by varying the shape and position of the obstacle.
Anyways, an analysis that aims to discuss the actual capability of the beams to recover requires an objective parameter, that relates the perturbed beam and the unperturbed one at a certain distance z from the lens. Furthermore, we wish the parameter to trace the same trend of reconstruction witnessed qualitatively in the simulations: it should be one before the obstacle, present a sadden downward jump at the obstruction plane, and grow constantly after it. We choose as a parameter the 2D correlation coefficient [21]. Given two matrices f and g, of dimension $N \cdot M$, that describe the intensity of the two fields, the correlation coefficient η is defined as follows:

$$\eta = \frac{\sum_{m=1}^{M}\sum_{n=1}^{N}\left[f_{m,n}-\overline{f}\right]\left[g_{m,n}-\overline{g}\right]}{\sqrt{\sum_{m=1}^{M}\sum_{n=1}^{N}\left[f_{m,n}-\overline{f}\right]^2\sum_{m=1}^{M}\sum_{n=1}^{N}\left[g_{m,n}-\overline{g}\right]^2}} \tag{2.1}$$

$$\overline{f} = \frac{\sum_{m=1}^{M}\sum_{n=1}^{N} f_{m,n}}{N \cdot M} \tag{2.2}$$

$$\overline{g} = \frac{\sum_{m=1}^{M}\sum_{n=1}^{N} g_{m,n}}{N \cdot M} \tag{2.3}$$

In order to understand if η has the desired trend, we evaluate it along the propagation of several obstructed beams.

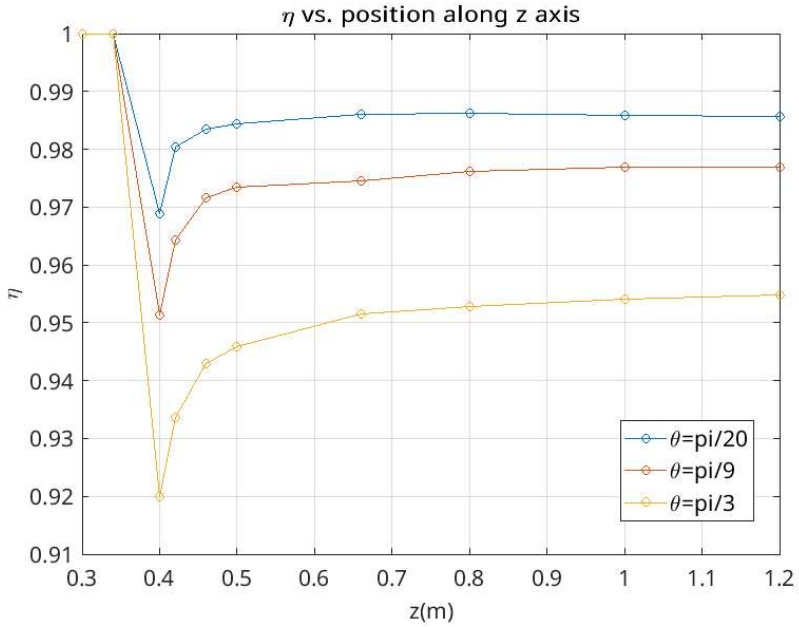

Figure 2.3: reconstruction parameter for a beam with parameters $n = -2$, $f = 20$ cm, $a = 2$ mm and $b = 3$ mm, obstructed by angular obstacles, symmetric with respect to the x axis that cut away the cusp region.

As desired, the parameter is 1 before the obstacle and immediately after it presents a growth, faster for smaller parameters and slower for larger ones, for which a smaller asymptotic value is reached. Now we look at how the parameter changes when we change the size of an obstacle. We use angular obstacles with different angles, placing them at the same distance along z, and evaluating the parameter at a distance for which it has reached a basically constant value that will be denoted η_f. We focus on

angular obstacles, and caustics with three cusps. In this case the size of the obstacle is modified via the parameter θ, that is its angular amplitude.

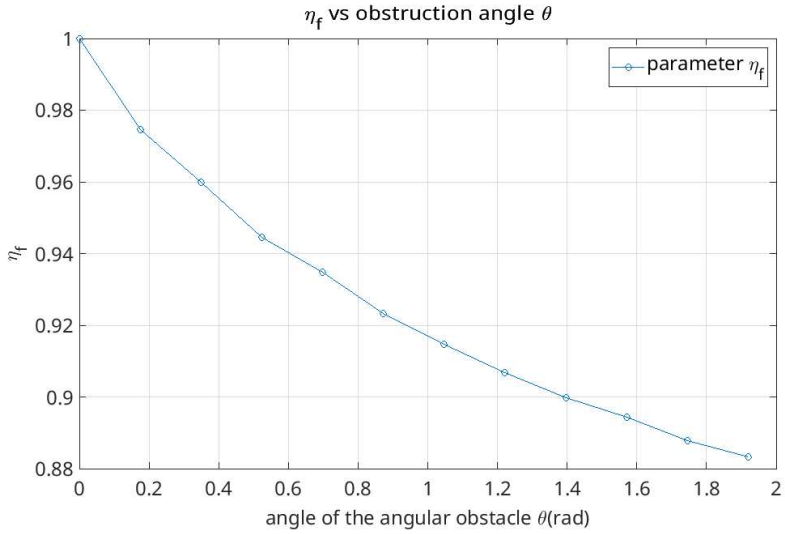

Figure 2.4: Values of η evaluated at $z = 5f$ for obstructions of increasing angle, placed at $z = 2f$, obstructing a beam characterised by $n = -2$, $f = 20$ cm, $a = 2$ mm and $b = 3$ mm

Chapter 3

Experimental analysis

3.1 DOE fabrication

To fabricate the optical elements we use gray-scale optical lithography with a positive photoresist. In order to apply this technique we use the uMLA (Heidelberg Instruments) for 3D lithography. The nanofabrication procedure converts a patter given by a 8-bit .BMP image, in this case representing a phase pattern, into a thin layer of material presenting regions of different thicknesses (128 available gray levels), allowing the fabrication of 3D textures of micro topographies. The textures are written on a glass substrate with a LED source ($\lambda = 365nm$), shaped by a DMD (digital micromirror device).

The fabrication procedure consists of several passages. First we prepare the substrate. We use as substrates microscope glass slides. The substrate needs to be cleaned from every sort of dust and impurity. The slide is initially blowed with compressed air, then is immersed inside a solution of 50ml of distilled water and 50ml iso-propanole (IPA). The next step is the spin coating. For this passage the slide is positioned in the spin platform, and a few drops of micro-resist $ma - P1225G$ (Micro Resist Technology) are poured on the top of it. The program needed for our purpose makes the slide rotate at 3000 rpm for 30 s, in this way the photoresist is spread over the substrate, forming a uniform thin layer of 2.5 μm. The next phase of the procedure is the soft-baking, where the solvants and bubbles can evaporate. This process consists in baking the slide at 95°C for 60 s. At this point the slide can be exposed to the UV radiation and it is placed inside the uMLA. We select the desired profile with the software, profiles are circular "bitmap" images of 5 mm of diameter and pixels of $2\mu m$ of side length. We select the job "Diffractive optics", that contains the series of operations that the uMLA will execute to fabricate the DOE. At this point we select the parameters that the uMLA will use for the fabrications. The key parameters are the defocusing, that we fix at 0 mm, and the exposure dose that we set at 4.05 mJ/cm^3, on the basis of the optimal recipe to fabricate diffractive optics working at 632.8 nm. The exposition to the UV radiation alters the photoresist, that is, it increments its solubility to the developer, the more in the zones that have been irradiated with a greater dose. After the resist film has been exposed it is now ready for the developement. The developement consists in pouring the developer, tetramethylammonium hydroxide(TMAH), over the slide and let it react with the photoresist for 60 s. In this way the final thickness of the resist will depend on the dose absorbed in every point by the material. Immediately after, it is necessary to clean the resist with distilled water, to stop the dissolution of the material. The water is than evaporated with the air-gun. The phase patterns to be reproduced are those in figure (1.1), in particular for $n = -2, -3$. A tilt was added to the original CST phase patterns, namely a constant gradient of the phase, because during the characterization of the optical elements a zero-order component of the input beam overlapped to the caustics to be observed. The tilt separates this undesired contribution from the caustic. The optical element generated can be observed at the uMLA via its optical microscope to verify that the target profile has been achieved (3.1).

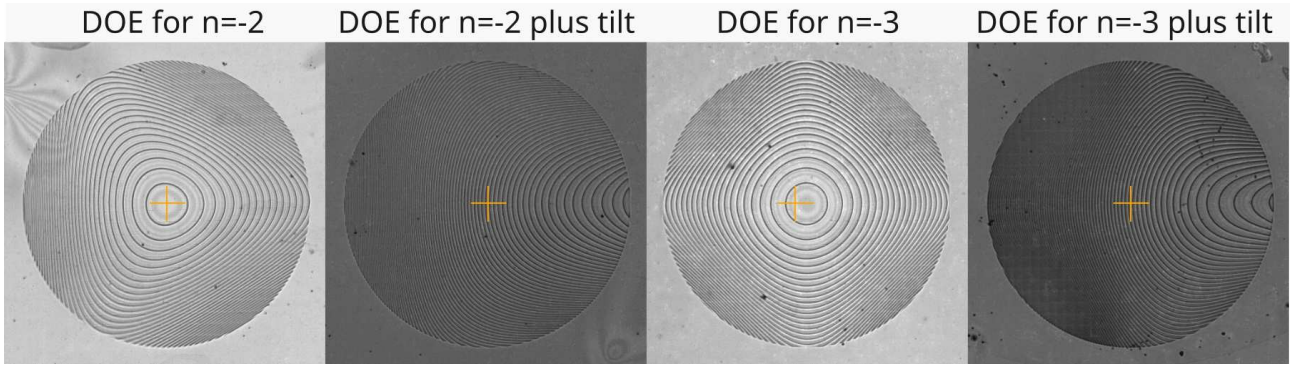

Figure 3.1: Acquisitions collected with the overview camera of the laser writer. The optical elements have a diameter of 5 mm. A tilt has been added to the pattern to separate a 0-order contribution due to imperfections, and avoid its overlap with the diffracted order.

3.2 Optical characterization

We proceed to characterise the diffractive optical elements with an experimental set-up on the optical table. The experiment, by visualizing the beam produced after the fabricated DOE, will validate the theoretical framework by comparing the real beams with the simulations. The source used is a laser HeNe (HNL008L, Thorlabs) producing light of wavelength of $\lambda = 632.8$ nm. The laser beam is firstly polarized horizontally, parallel to the worktop (Figure 3.2). Then it is widen, by means of two lenses (indicated as L_1 and L_2) of focal length $f_1 = 2.54$ cm and $f_2 = 15.00$ cm, acting as a telescope and producing a magnification of 6. The ray obtained passes through a 50:50 beam-splitter (BS) (CM1-BS013, Thorlabs). In front of the beam-splitter is positioned a liquid-crystals-on-silicon (LCoS) spatial light modulator (SLM) (PLUTO-NIR-010-A, Holoeye) (Figure 3.3). The spatial light modulator, and the lenses positioned between it (referred to as L_3, $f_3 = 20$ cm and L_4, $f_4 = 25$ cm) and the DOE, are needed to create a Gaussian beam of waste $w_0 = 2.5$ mm (Figure 3.4). At this point the Gaussian beam is directed toward the optical element. Beyond the optical element we can finally perform a measurement of the intensity profile of the beam by means of a CMOS camera (CDD 1545M, Thorlabs), producing images of 1280x1024 pixels for which 1 pixel is equal to 5.2 μm. In the following images are presented the experimental results compared with the simulated theoretical model of the caustics. For both the deltoid and the astroid the theoretical models are in well agreement with the size of the caustic beams.

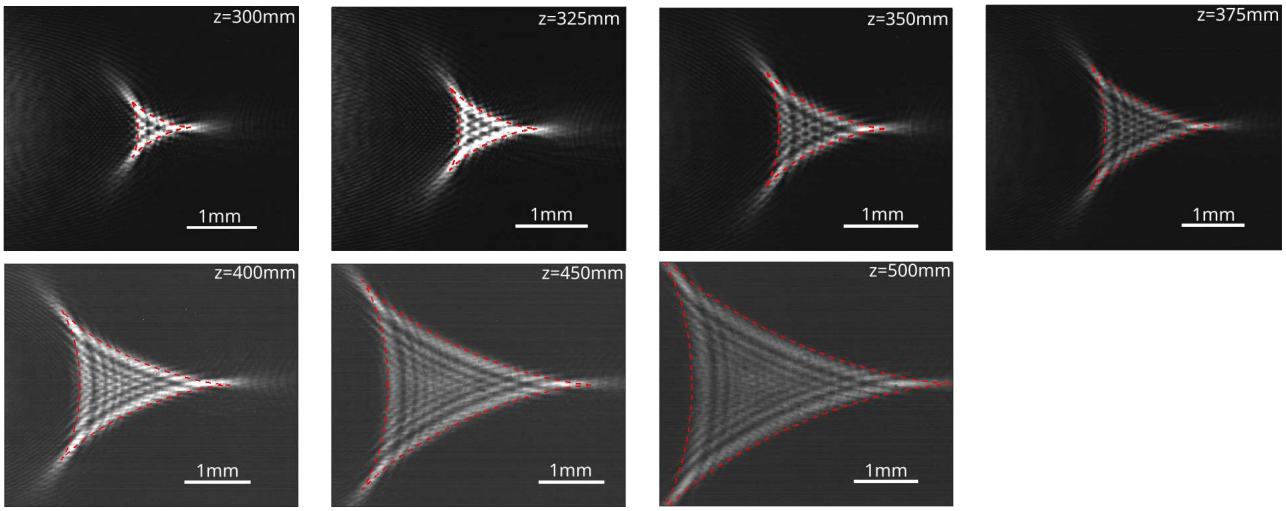

Table 3.1: CMOS camera images of the intensity profile of the caustic beam with $n = -2$, $f = 20$ cm, $a = 2$ mm and $b = 3$ mm propagated through the DOE and compared with the theoretical model, represented by the red dotted line.

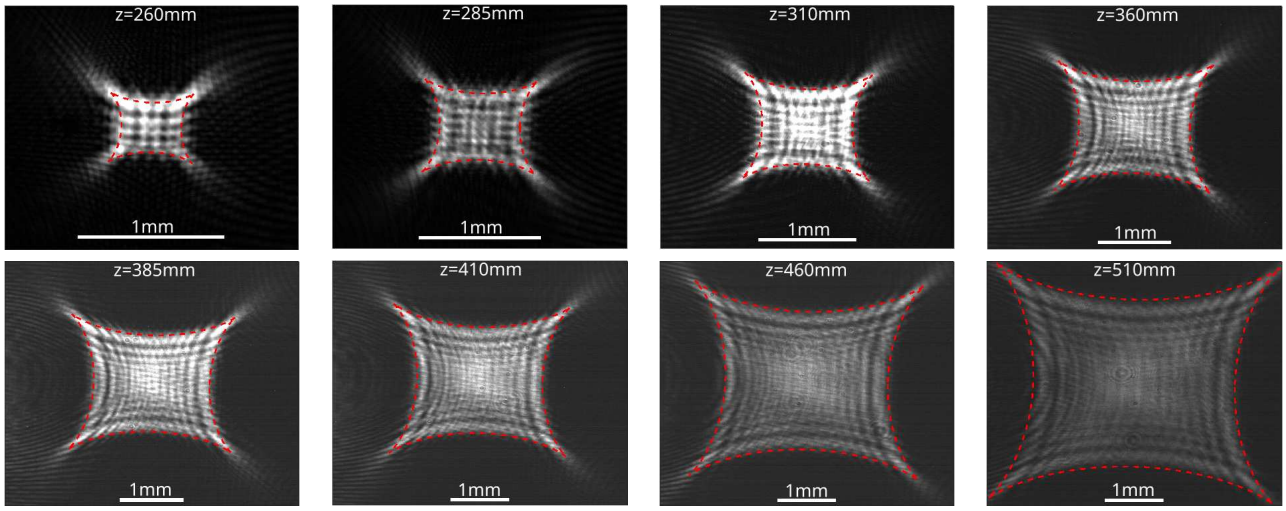

Table 3.2: CMOS camera images of the intensity profile of the caustic beam with $n = -3$, $f = 20$ cm, $a = 2$ mm and $b = 3$ mm propagated through the DOE and compared with the theoretical model, represented by the red dotted line.

3.3 Self-healing experimental results

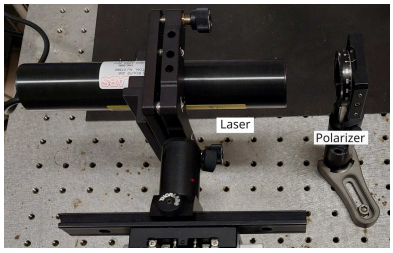

Figure 3.2: The laser beam (632.8 nm) is polarized parallel to the optical table

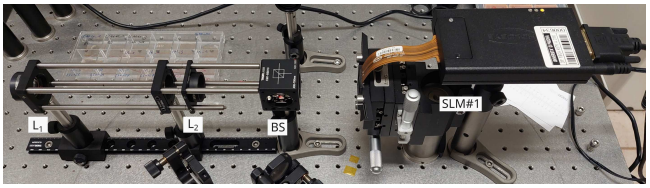

Figure 3.3: The beam is magnified by the sequence of the bi-convex lenses L_1 and L_2, $f_1 = 2.54$ cm, $f_2 = 15$ cm, crosses the beam-splitter (BS), and gets shaped by spatial light modulator (SLM#1), as a first step to produce the Gaussian beam.

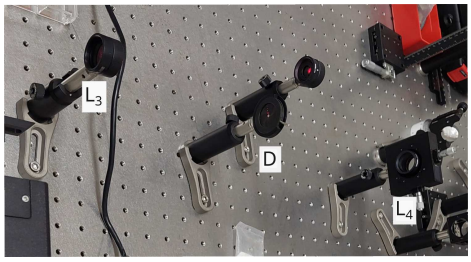

Figure 3.4: After the beam has been reflected by the spatial light modulator, SLM#1, it passes through the bi-convex lenses L_3, L_4, $f_3 = 20$ cm, $f_4 = 25$ cm, and the diaphragm(D), to produce the Gaussian beam of $w_0 = 2.5$ cm.

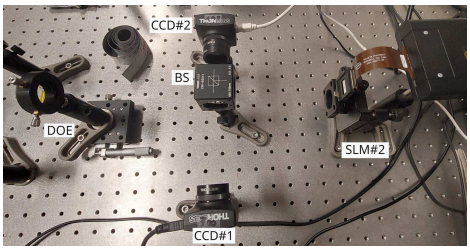

Figure 3.5: The beam passes through the DOE forming the caustic, that is detected unperturbed by the camera CCD#1. The beam is perturbed by the SLM#2, the unperturbed beam is detected by the camera CCD#2

Starting from the setup of the optical characterization, now a beam-splitter(BS) is placed after the optical element. One beam is detected by a CCD camera, while the other is sent to a second SLM, that is used to generate the obstruction. Since the SLM works reflecting the beam and modifying its phase with patterns given by 8-bit images, the part of the caustic that shouldn't encounter the obstacle is reflected back to the beam-splitter, while a tilt is added to the area of the beam that should be blocked, separating it from the main beam. The perturbed caustic that goes back to the beam-splitter is then revealed by an other CCD camera (Figure 3.5).

The first obstructions analysed are circles of increasing radius:

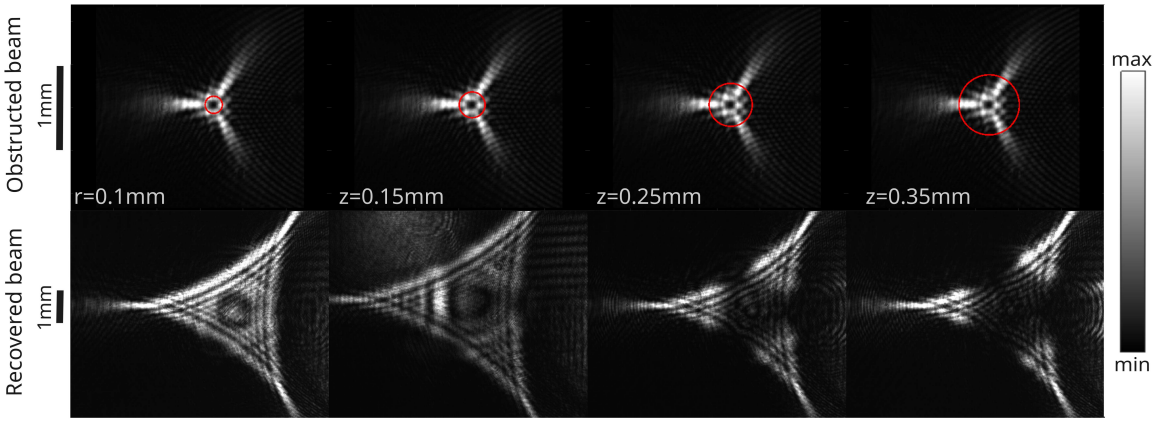

Figure 3.6: Caustics with $n = -2$, $f = 20$cm, $a = 2$ mm and $b = 3$ mm, obstructed by angular obstacles. The obstacles are placed at 22 cm from the DOE, while the reconstructed beam is revealed at 53 cm from the DOE. The beam being obstructed is shown in the top row, where the area contained by the red lines is the region removed by the obstacle. The recovered beam is shown in the bottom row.

Now angular obstructions are considered:

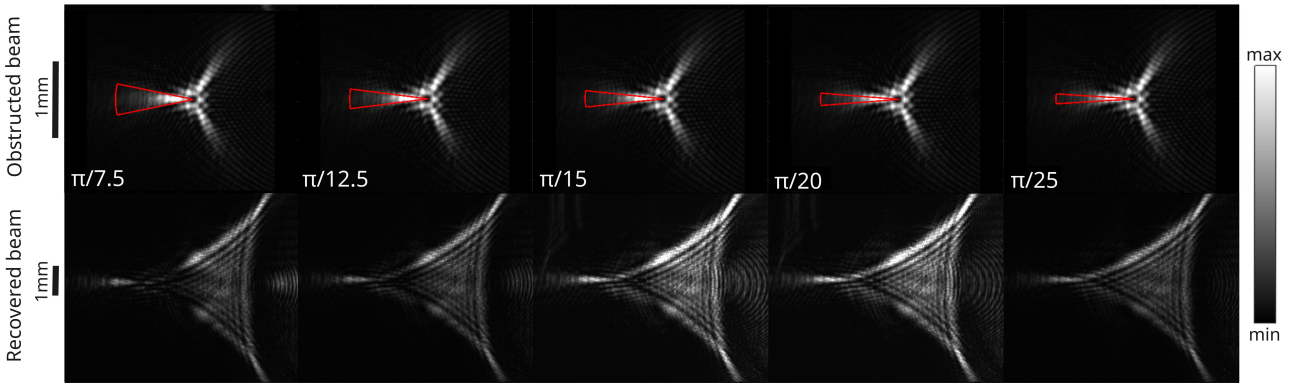

Figure 3.7: Caustics with $n = -2$, $f = 20$ cm, $a = 2$ mm and $b = 3$ mm, obstructed by angular obstacles. The obstacles are placed at 22 cm from the DOE, while the reconstructed beam is revealed at 53 cm from the DOE. The beam being obstructed is shown in the bottom row, where the area contained by the red lines is the region removed by the obstacle. The recovered beam is shown in the upper row.

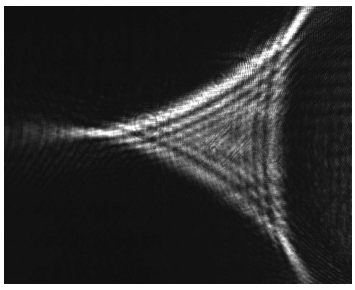

Figure 3.8: Unobstructed beam at $z = 53$ cm

From images (3.6,3.7) it is visible the effect of the self-healing ability of regular polygon beams. When considering angular obstacles the cusp that is taken away completely by the obstacle reappears, while for the same set of obstructions the internal pattern is less reconstructed when increasing constantly the angle of the beam. The internal bright region is considered in greater detail in the case of circular obstacles, where even for a radius of $r = 0.25$ mm that takes away the all body of the cusp, this region is visible even if with a lower intensity.

Chapter 4

Conclusions and discussions

We have studied the property of self-healing for regular polygon caustic beams, that present hypocycloid caustic envelopes, with accelerating cusps along the propagation axis. We focused mainly on deltoids, with three cusps, and the astroids, having four cusps. These beams also present a bright internal region, where a greater concentration of rays is conveyed, characterized by a typical interference pattern with luminous fringes. The caustics have been blocked with angular obstacles of varying angular amplitude, and with circular obstacles of increasing radius. The approach is that of observing the regeneration of the beams ranging from small obstructions, representing a slight perturbation of the field, to obstacles of increasing sizes. The degradation of the field ranges from a small perturbation of the intensity and position of the luminous fringes, to the disruption of these patterns for bigger obstacles. We also observe that the regeneration is not uniform over the cross sections, and the cusps are particularly robust, even for obstacles that subtract great internal portions of the beams. To quantitatively describe the amount of regeneration of the beam, we have introduced the 2D correlation coefficient as a parameter that compares the unobstructed beam, and the beam being perturbed. That has revealed itself as a useful and valid tool to confront the degree of self-healing of a beam, as its trend is coherent with the level of regeneration of the beam structure that we observe qualitatively. Furthermore, the accordance between the simulations and the beam produced with the fabricated DOE has validated the results of the simulations itself, that we have used to predict and study the self healing, and the theoretical framework based on the conformal transformation, as well as the theoretical model developed from the stationary phase approximation. The robustness of the caustic beams under the obstruction with an obstacle is interesting for several applications.

In free space optical communication (FSO), self-healing and regular polygon caustics could be exploited to make a light beam travel for a longer distance in a turbulent medium without being significantly distorted and limiting the random phase and intensity fluctuations, or make it travel beyond an obstacle with reduced distortion. Also, the cross-talk between different spatially multiplexed channels could be mitigated, increasing the quality of the signal, and the channels efficiency [3].

In light-sheet fluorescence microscopy (LSFM) imaging, a self-healing beam could be exploited, thanks to its ability to maintain its profile for deeper distances in thick biological samples, for example skin or brain tissue, to increase the image contrast [12].

In optical tweezers and optical trapping, that represent powerful and non-invasive tools to manipulate small particles thanks to the light-matter interaction, the exploitation of self-healing can be useful to trap and control particles or cells in a single longitudinal axis, for the ability of the beam to regenerate after the particles to be controlled [22], [4], enabling for example to manipulate particles or cells in separated samples, or to create polygonal channels where to make the particles travel, accelerate, or being trapped [23].

Bibliography

[1] R. MacDonald, S. Boothroyd, T. Okamoto, J. Chrostowski, and B. Syrett, "Interboard optical data distribution by bessel beam shadowing," *Optics Communications*, vol. 122, no. 4, pp. 169–177, 1996.

[2] Z. Bouchal, J. Wagner, and M. Chlup, "Self-reconstruction of a distorted nondiffracting beam," *Optics Communications*, vol. 151, no. 4, pp. 207–211, 1998.

[3] S. Li and J. Wang, "Adaptive free-space optical communications through turbulence using self-healing bessel beams," *Scientific Reports*, vol. 7, p. 43233, 02 2017.

[4] V. Garces, D. Mcgloin, H. Melville, W. Sibbett, and K. Dholakia, "Simultaneous micromanipulation in multiple planes using a self-reconstructing light beam," *Nature*, vol. 419, pp. 145–7, 10 2002.

[5] Y. Zhou, w. Gaofeng, Y. Cai, F. Wang, and B. Hoenders, "Application of self-healing property of partially coherent beams to ghost imaging," *Applied Physics Letters*, vol. 117, p. 171104, 10 2020.

[6] Y. Shen, S. Pidishety, I. Nape, and A. Dudley, "Self-healing of structured light: a review," *Journal of Optics*, vol. 24, p. 103001, sep 2022.

[7] J. Broky, G. A. Siviloglou, A. Dogariu, and D. N. Christodoulides, "Self-healing properties of optical airy beams," *Opt. Express*, vol. 16, pp. 12880–12891, Aug 2008.

[8] J. D. Ring, J. Lindberg, A. Mourka, M. Mazilu, K. Dholakia, and M. R. Dennis, "Auto-focusing and self-healing of pearcey beams," *Opt. Express*, vol. 20, pp. 18955–18966, Aug 2012.

[9] P. Zhang, Y. Hu, T. Li, D. Cannan, X. Yin, R. Morandotti, Z. Chen, and X. Zhang, "Nonparaxial mathieu and weber accelerating beams," *Phys. Rev. Lett.*, vol. 109, p. 193901, Nov 2012.

[10] G. Ruffato, S. Brunetta, and H. Kobayashi, "A general conformal framework for regular cusp beams," *Optics Communications*, vol. 517, p. 128325, 2022.

[11] Z. Zheng, B. Zhang, H. Chen, J. Ding, and H.-T. Wang, "Optical trapping with focused airy beams," *Applied optics*, vol. 50, pp. 43–9, 01 2011.

[12] S. Jia, J. Vaughan, and X. Zhuang, "Isotropic 3d super-resolution imaging with a self-bending point spread function," *Nature Photonics*, vol. 8, 03 2014.

[13] M. Born, E. Wolf, A. B. Bhatia, P. C. Clemmow, D. Gabor, A. R. Stokes, A. M. Taylor, P. A. Wayman, and W. L. Wilcock, "Principles of optics: Electromagnetic theory of propagation, interference and diffraction of light," 1999.

[14] J. Goodman, "Introduction to fourier optics," 2005.

[15] J. Li, Z. Peng, and Y. Fu, "Diffraction transfer function and its calculation of classic diffraction formula," *Optics Communications*, vol. 280, no. 2, pp. 243–248, 2007.

[16] D. Wang, A. Pe'er, A. A. Friesem, and A. W. Lohmann, "General linear optical coordinate transformations," *J. Opt. Soc. Am. A*, vol. 17, pp. 1864–1869, Oct 2000.

[17] Y. A. Kravtsov and Y. I. Orlov, "Caustics, catastrophes, and wave fields," *Soviet Physics Uspekhi*, vol. 26, p. 1038, dec 1983.

[18] W. Liu, Y. Zhang, J. Gao, and X. Yang, "Generation of three-dimensional optical cusp beams with ultrathin metasurfaces," *Scientific Reports*, vol. 8, 06 2018.

[19] M. Malik, M. O'Sullivan, B. Rodenburg, M. Mirhosseini, J. Leach, M. P. J. Lavery, M. J. Padgett, and R. W. Boyd, "Influence of atmospheric turbulence on optical communications using orbital angular momentum for encoding," *Opt. Express*, vol. 20, pp. 13195–13200, Jun 2012.

[20] M. Anguiano-Morales, A. Martínez, M. D. Iturbe-Castillo, S. Chávez-Cerda, and N. Alcalá-Ochoa, "Self-healing property of a caustic optical beam," *Appl. Opt.*, vol. 46, pp. 8284–8290, Dec 2007.

[21] N. Hermosa, C. Rosales-Guzmán, and J. P. Torres, "Helico-conical optical beams self-heal," *Opt. Lett.*, vol. 38, pp. 383–385, Feb 2013.

[22] J. Arlt, V. Garces-Chavez, W. Sibbett, and K. Dholakia, "Optical micromanipulation using a bessel light beam," *Optics Communications*, vol. 197, no. 4, pp. 239–245, 2001.

[23] J. Park, S. Hong, Y. Lee, H. Lee, S. Kim, K. Dholakia, and K. Oh, "Optical manipulation of a dielectric particle along polygonal closed-loop geometries within a single water droplet," *Scientific Reports*, vol. 11, p. 12690, 06 2021.